Subtle blood-brain barrier leakage rate and spatial extent

Subtle blood-brain barrier leakage rate and spatial extent: Considerations for dynamic contrast-enhanced MRI

Harm J. van de Haar
Department of Radiology and Nuclear Medicine, Maastricht University Medical Center, PO box 5800, Maastricht 6202 AZ, The Netherlands
Department of Neuropsychology and Psychiatry/Alzheimer Center Limburg, Maastricht University Medical Center, PO box 616, Maastricht 6200 MD, The Netherlands
School for Mental Health and Neuroscience, Maastricht University, PO box 616, Maastricht 6200 MD, The Netherlands

Jacobus F.A. Jansen
Department of Radiology and Nuclear Medicine, Maastricht University Medical Center, PO box 5800, Maastricht 6202 AZ, The Netherlands
School for Mental Health and Neuroscience, Maastricht University, PO box 616, Maastricht 6200 MD, The Netherlands

Cécile R.L.P.N. Jeukens
Department of Radiology and Nuclear Medicine, Maastricht University Medical Center, PO box 5800, Maastricht 6202 AZ, The Netherlands

Saartje Burgmans
Department of Neuropsychology and Psychiatry/Alzheimer Center Limburg, Maastricht University Medical Center, PO box 616, Maastricht 6200 MD, The Netherlands
School for Mental Health and Neuroscience, Maastricht University, PO box 616, Maastricht 6200 MD, The Netherlands

Mark A. van Buchem
Department of Radiology, Leiden University Medical Center, PO box 9600, Leiden 2300 RC, The Netherlands

Majon Muller
Department of Gerontology and Geriatrics, Leiden University Medical Center, PO box 9600, Leiden 2300 RC, The Netherlands

Paul A.M. Hofman
Department of Radiology and Nuclear Medicine, Maastricht University Medical Center, PO box 5800, Maastricht 6202 AZ, The Netherlands
School for Mental Health and Neuroscience, Maastricht University, PO box 616, Maastricht 6200 MD, The Netherlands

Frans R.J. Verhey
Department of Neuropsychology and Psychiatry/Alzheimer Center Limburg, Maastricht University Medical Center, PO box 616, Maastricht 6200 MD, The Netherlands
School for Mental Health and Neuroscience, Maastricht University, PO box 616, Maastricht 6200 MD, The Netherlands

Matthias J.P. van Osch
Department of Radiology, Leiden University Medical Center, PO box 9600, Leiden 2300 RC, The Netherlands

Walter H. Backes[a)]
Department of Radiology and Nuclear Medicine, Maastricht University Medical Center, PO box 5800, Maastricht 6202 AZ, The Netherlands
School for Mental Health and Neuroscience, Maastricht University, PO box 616, Maastricht 6200 MD, The Netherlands

(Received 2 August 2016; revised 29 March 2017; accepted for publication 17 April 2017; published 10 July 2017)

Purpose: Dynamic contrast-enhanced (DCE) MRI can be used to measure blood-brain barrier (BBB) leakage. In neurodegenerative disorders such as small vessel disease and dementia, the leakage can be very subtle and the corresponding signal can be rather noisy. For these reasons, an optimized DCE-MRI measurement and study design is required. To this end, a new measure indicative of the spatial extent of leakage is introduced and the effects of scan time and sample size are explored.
Methods: Dual-time resolution DCE-MRI was performed in 16 patients with early Alzheimer's disease (AD) and 17 healthy controls. The leakage rate (K_i) and volume fraction of detectable leaking tissue (v_L) to quantify the spatial extent of BBB leakage were calculated in cortical gray matter and white matter using noise-corrected histogram analysis of leakage maps. Computer simulations utilizing realistic K_i histograms, mimicking the strong effect of noise and variation in K_i values, were performed to understand the influence of scan time on the estimated leakage.
Results: The mean K_i was very low (order of 10^{-4} min^{-1}) and highly influenced by noise, causing the K_i to be increasingly overestimated at shorter scan times. In the white matter, the K_i was not different between patients with early AD and controls, but was higher in the cortex for patients, reaching significance after 14.5 min of scan time. To detect group differences, v_L proved more suitable,

showing significantly higher values for patients compared with controls in the cortex after 8 minutes of scan time, and in white matter after 15.5 min.

Conclusions: Several ways to improve the sensitivity of a DCE-MRI experiment to subtle BBB leakage were presented. We have provided v_L as an attractive and potentially more time-efficient alternative to detect group differences in subtle and widespread blood-brain barrier leakage compared with leakage rate K_i. Recommendations on group size and scan time are made based on statistical power calculations to aid future research. © *2017 American Association of Physicists in Medicine* [https://doi.org/10.1002/mp.12328]

Key words: Alzheimer's disease, blood-brain barrier, brain MRI, dynamic contrast-enhanced MRI, leakage, pharmacokinetic modeling

1. INTRODUCTION

Impairment of the blood-brain barrier (BBB) is thought to be a key mechanism in the pathophysiology of several brain diseases such as small vessel disease, Alzheimer's disease (AD) and multiple sclerosis.[1–4] A suitable method to investigate this impairment is dynamic contrast-enhanced (DCE) MRI, which is a noninvasive imaging technique that follows the arrival and distribution of a contrast agent over time. The most common contrast agents in MRI are gadolinium-based compounds, which almost completely remain intravascular in a healthy brain due to the BBB.[5,6] The BBB is a collection of anatomical elements in the wall of brain capillaries. It protects the neuronal tissue from neurotoxic compounds, while allowing essential molecules such as oxygen or nutrients to pass. When damaged, certain substances can pass the BBB more easily, which may be harmful to the brain parenchyma. In case of pathology, such as (high-grade) tumors or infarctions, microvessels become hyperpermeable and the contrast agent may extravasate more easily and accumulate in the brain parenchyma. This leakage can be detected, and the difference between intravascular and extravascular contrast agent concentration can be quantified using DCE-MRI.[7] However, compared to high-grade tumors and infarcted brain tissue, the leakage in neurodegenerative disorders such as Alzheimer's disease is found to be very subtle, making it much more difficult to discriminate between intra- and extravascular contrast agent.[8–10] Furthermore, the spatial extent and distribution of the leakage is also of interest. Contrary to tumors, the leakage in a neurodegenerative disease may not be localized at an obvious site, making detection of the leakage within a large region more important. *A priori*, it remains unknown what better characterizes the BBB damage in a neurodegenerative disease; the magnitude of the leakage rate or the spatial extent of the leakage. Furthermore, investigating this also requires a more sensitive technique compared with tumors, as the leakage is orders of magnitude lower in the brain tissue and difficult to distinguish from noise.

To measure such subtle diffuse leakage, the DCE-MRI methodology has to be further modified to detect low concentrations of contrast agent and slower signal changes over time. Previous studies have looked at the most optimal pharmacokinetic model and the ability to distinguish low leakage from zero.[6,11] However, improving the DCE-MRI experiment to voxelwise mapping of the leakage remains difficult. A straightforward way to improve the sensitivity for subtle leakage is to scan longer, which increases the amount of data points from which leakage can be estimated, and also allows the contrast agent more time to extravasate and accumulate in the tissue, increasing the range of intensity values. In the majority of studies which apply DCE-MRI in neurodegenerative diseases, a protocol of roughly 20–30 min is used, although some recent studies use shorter protocols of 16 min.[6,9,10,12–15] In a group study, the sensitivity to subtle leakage can also be improved by increasing the group sizes. Additionally, the analysis method can be further improved, reducing the impact of noise on the leakage quantification.

The aim of this study is to explore several ways to improve the ability to detect widespread subtle BBB leakage in neurodegenerative diseases. First, we explore the effect of changing the acquisition time on the measured leakage. Second, to determine the spatial extent of the lowest possible leakage rates, we propose a noise removal method and the alternative leakage measure "volume fraction of detectable leaking brain tissue voxels" (v_L), which may help to distinguish very low leakage from noise. We further investigated this using data from *in vivo* DCE-MRI measurements in patients with early AD and healthy age-matched controls. To obtain more insight into the relation between scan time and measurement of subtle BBB leakage, computer model simulations were implemented, using representative leakage rate (K_i) histograms that mimic the effect of voxelwise mapping of the leakage measures with *in vivo* noise and realistic variations in measured K_i values. In addition, we investigated the scan time and group size necessary to detect significant group differences, which may assist to motivate the best study design for future DCE-MRI studies. Data from both the white matter and the cortical gray matter are reported, as different requirements are expected for tissues with different degrees of vascularization. Recently, the differences in cerebral leakage between patients with early AD and healthy elderly subjects were published using the same *in vivo* data set (Ref. [16]). With the use of this data set and additional computer simulations we set out to critically analyze the applied method, the effect of scan time, noise, and sample size on the leakage measures.

2. MATERIALS AND METHODS

2.A. Imaging: subjects

Sixteen patients with early AD (mean age 73.6 s.d. 7.9 yr, 7 women), defined as being diagnosed with either mild dementia of the AD type or mild cognitive impairment due to AD, and 17 healthy age-matched controls (mean age 75.8 s.d. 6.2 yr, 6 women) were included. All subjects underwent MRI at the Maastricht University Medical Center or Leiden University Medical Center. Subjects were excluded in case of contraindications for MRI, renal dysfunction, major structural brain abnormalities, alcohol/drug abuse, or other major vascular, psychiatric or neurological disorders. This study was approved by both the Medical Ethical Committee AZM/UM and the Committee for Medical Ethics LUMC. Informed consent was obtained from all patients after they received verbal and written descriptions of the study.

2.B. Imaging: MRI protocol

To detect BBB leakage, a dual time resolution dynamic contrast-enhanced imaging protocol was implemented for 3T MRI (Achieva, Philips Healthcare, Best, The Netherlands). This protocol consisted of two nested pulse sequences, a slow and a fast sequence. This approach is comparable to the imaging protocol employed by Jelescu et al., which was found to be more precise and less biased at estimating BBB impairment in multiple sclerosis, compared with a conventional single time resolution scan, and was also found to be relatively insensitive to variations in perfusion levels.[17] Figure 1 illustrates the time-course of the various acquisition parts of the dual time resolution scan protocol. The slow sequence started immediately after the fast sequence, for a total time of 25 min, including three precontrast (slow sequence) volumes which are needed for further analysis. All reported scan times include these three precontrast scans, the fast sequence and the postcontrast slow sequence volumes. In the dual time resolution scan, the fast sequence allowed for a higher temporal resolution during initial arrival and recirculation of the contrast agent, while the slow sequence provided a better SNR, but lower temporal resolution during contrast agent distribution and washout. Both sequences are based on a previously described sequence, for which the relation between signal and longitudinal relaxation rate is known and can be used for longitudinal relaxation time T_1 mapping.[5] The fast sequence was a saturation recovery 3D gradient recalled sequence (TR/TE 5.2/2.5 ms, flip angle 30°, 25.6 × 20 × 5 cm^3 FOV), 256 × 200 × 10 matrix, dynamic scan interval (DSI) 3.2 s) with a saturation prepulse given at a delay time (TD) of 120 ms, used during bolus injection (gadobutrol, 0.1 mmol/kg) for 1.5 min. The slow sequence was also a saturation recovery gradient recalled sequence (TR/TE 5.6/2.5 ms, 25.6 × 25.6 × 10 cm^3 FOV, 256 × 256 × 50 matrix, DSI 30.5 s) with the same prepulse. The two sequences were combined by spatially interpolating the 5-mm thick slices of the fast sequence to the spatially match (i.e., upsampling) the 2-mm thick slices of the slow scan. Because the sequences were combined on the MRI console, the time indices of each slow and fast volume relative to the start of the DCE-MRI sequence were present in the exported data. T_1 weighted structural images were used for automated and manually adjusted tissue classification into white matter (WM) and gray matter (GM) using the FreeSurfer software package (version 5.1.0).[18] A fluid attenuated inversion recovery (FLAIR) scan was used to segment white matter hyperintensities, which were excluded from the WM mask to create the normal appearing white matter (NAWM) mask.[19]

2.C. Leakage analysis

The sequential images underwent correction for head displacement using a mutual information algorithm with an averaged precontrast image as reference (FLIRT, the linear image registration tool of the Oxford Centre for functional MRI of the brain (FMRIB), fsl.fmrib.ox.ac.uk/fsl/fslwiki/FLIRT). An individual vascular input function (VIF) was extracted per participant from the superior sagittal sinus, also used by others.[17,20–22] We used individual VIFs in this study with elderly subjects as it is known that cerebral blood flow may depend on age, especially in subjects with neurodegenerative diseases. The VIF was chosen from the superior sagittal sinus as it could be easily identified in each subject's field of view, had a sufficient number of voxels that were for 100% filled with (contrast-enhanced) blood, and did not show high-flow signal contamination due to the relatively slow blood velocity in comparison to the arterial blood stream. The intra-cerebral arteries, on the other hand, could not be identified in all subjects and had too small sizes to avoid partial volume artifacts. To obtain the signal time-courses of the VIF regions-of-interest were drawn in the lumina of the superior sagittal sinus in the most central slices of the 3D fast scan volumes.

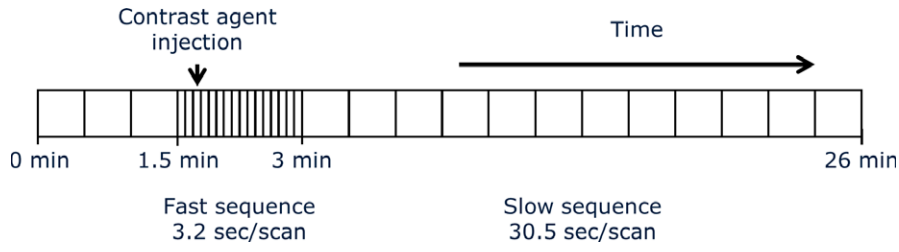

FIG. 1. The time course of the various acquisition parts and contrast agent administration of the dual time resolution magnetic resonance scan protocol. [Color figure can be viewed at wileyonlinelibrary.com]

Further analysis was performed using in-house developed software implemented in Matlab (MathWorks, Natick, MA, USA). Signal time-courses were first temporally processed using a Savitsky-Golay kernel to smooth the noisy time-courses but preserving steeper signal changes due to contrast agent wash-in and wash-out. Translation of the signal enhancement to contrast agent concentration was performed in two ways. For the VIF, the signal enhancement was converted to the contrast agent concentration using *in vitro* concentration calibrations. These calibrations were performed using a diluted $MnCl_2$ stock solution with a baseline T_1 of 1650 ms, which is comparable to human blood. The signal change caused by different gadobutrol concentrations (1–40 mM) in the stock solution was measured for both the fast and the slow sequence. For the brain tissue, the expectedly low contrast agent concentration was calculated assuming a linear relationship between signal change and contrast agent concentration and using a contrast agent relaxivity of 3.3 s^{-1} mM^{-1}.[16,23] Compared with the nonlinear relation between signal intensity and contrast agent concentration, the linear approximation showed a 2% discrepancy at 0.2 mM, which is on the high end of the concentrations typically found in tissue. The longitudinal relaxation times, prior to contrast agent enhancement, T_{10} were obtained using a sequence comparable to the slow sequence but with different TD settings (120–4000 ms).[5] The mean T_{10} values for the tissue of the subjects was calculated, and the individual segmentations of the T_1 structural scans were used to assign voxelwise T_{10} values to the WM and GM. These T_{10} maps were smoothed with a $2 \times 2 \times 2$ mm kernel to account for partial volume effects of the tissue. Next, a two-compartment pharmacokinetic model was applied voxel-wise, using the Patlak graphical approach.[24] The Patlak plot provided the BBB leakage rate (K_i, in min^{-1}) from the slope, and the fractional blood plasma volume (v_p) from the intercept (assuming a hematocrit level of 45%). The v_p was not further investigated in this study as it was mainly dependent on the data from the fast DCE-MRI sequence, and appeared relatively insensitive to the total scan time including the slow sequence.[25] The median K_i of all voxels within the NAWM and GM per subject was calculated, which is for simplicity referred to as leakage rate K_i for the remainder of this article.

2.D. Noise correction and fractional volume of leaking tissue calculation

Due to noise on the concentration time curves, the slope of the Patlak plot had values that fluctuates around zero and were occasionally positive, zero but also negative. However, a K_i value smaller than zero is physiologically meaningless. Therefore, we assumed that all negative K_i values were caused by noise on the concentration time curves. Keep in mind that only part of the positive Ki values are physiological while others, especially those close to zero, may also represent noise. A noise on top of the signal in a non- (or negligibly-) leaking voxel would equally likely result in a negative as well as a positive K_i, we also assumed that the noise would give rise to an equal distribution on the positive side. Note that this noise is from the K_i distribution which is calculated from the dynamic MRI measurements, which originates from but is conceptually different from the noise on the directly recorded MRI signal time-courses. Computer simulations (see section Simulations) using model concentration time-courses of brain tissue enhancement and a vascular input function and the Patlak approach confirmed that the noise in the K_i histogram was highly symmetric around K_i=0 when the input K_i value was zero. Further investigation of the observed *in vivo* K_i histograms showed that the distribution was skewed towards the upper tail containing high K_i values, which we consider to be likely due to actual leakage instead of noise. By mirroring the negative bins to the positive side, the total noise was estimated and subsequently removed from the histograms. The bins remaining after noise correction were considered to represent the distribution of voxels that exhibit detectable leakage (Fig. 2). Note that the bins remaining after noise removal do not represent the complete distribution of the leaking brain tissue, but only the detectable part. In this way, neither K_i values nor voxels are classified as noise or leakage, but this method allows for the calculation of histogram measures of the leakage. The cumulative sum of the resulting bins was defined to represent the detectable fractional volume of leaking tissue: v_L. Therefore, v_L is a measure of the fraction of voxels that exhibit a detectable leakage in an ROI. A higher v_L would indicate an increase of voxels showing leakage. A higher K_i would indicate a stronger overall leakage. This procedure was also employed in a previous study.[16] An example to illustrate the difference between K_i and v_L is displayed in Fig. 3, which shows two leakage distributions with roughly equal average K_i values but a very different v_L. In Fig. 4 it is illustrated how different input distributions with varying fractions of nonleaking ($K_i = 0$) and leaking ($K_i > 0$) voxels, with varying leakage rate, result in noisy output histograms. It also demonstrates how v_L is able to differentiate nonleaking from leaking voxels, and how altering the leakage rate and proportion of leaking voxels affects the mean K_i and v_L. It is furthermore noted that a histogram analysis does not utilize spatial information and as white and grey matter have different degrees of vascularization, which is why the analysis was detailed to white and grey matter separately.

One of the aims of this study is to provide information on how to improve the experimental setup of future studies. To facilitate easy comparisons between this study and previous DCE-MRI studies, all tissue K_i values reported in this study were calculated from the full (uncorrected) histogram, while vL was calculated from the noise-corrected histogram. The noise suppression method is only utilized to calculate the v_L, and any K_i mentioned in this study is based on the raw (and noisy) values.

2.E. Statistical analysis

A two-sided Student's t-test was used to determine significant differences in median K_i of the full histogram and v_L of the noise-corrected histogram between patients and controls

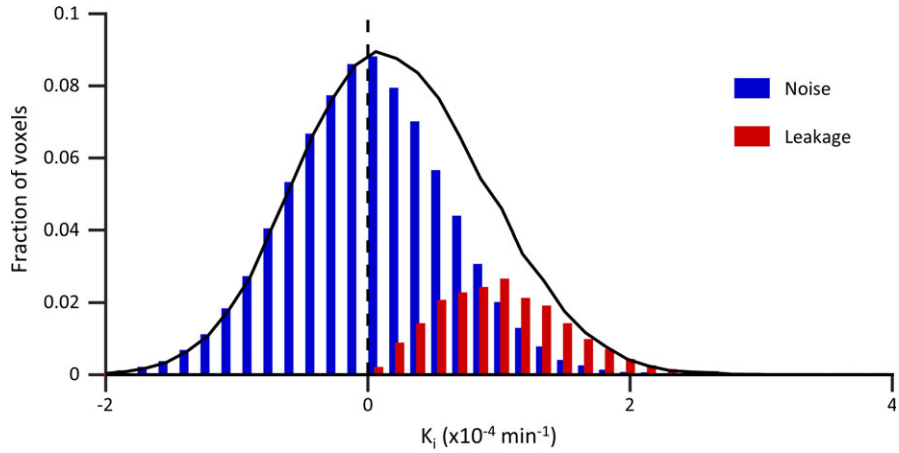

FIG. 2. A schematic overview of the histogram method. The shape of the total (measured) histogram is displayed as a black line. By assuming that all bins with negative K_i values are due to noise, the noise in the positive bins can be estimated by mirroring the negative bins to the positive side, which are displayed as the blue bins. The remaining bins, which are displayed in red, are then assumed to exhibit leakage that can be differentiated from noise.

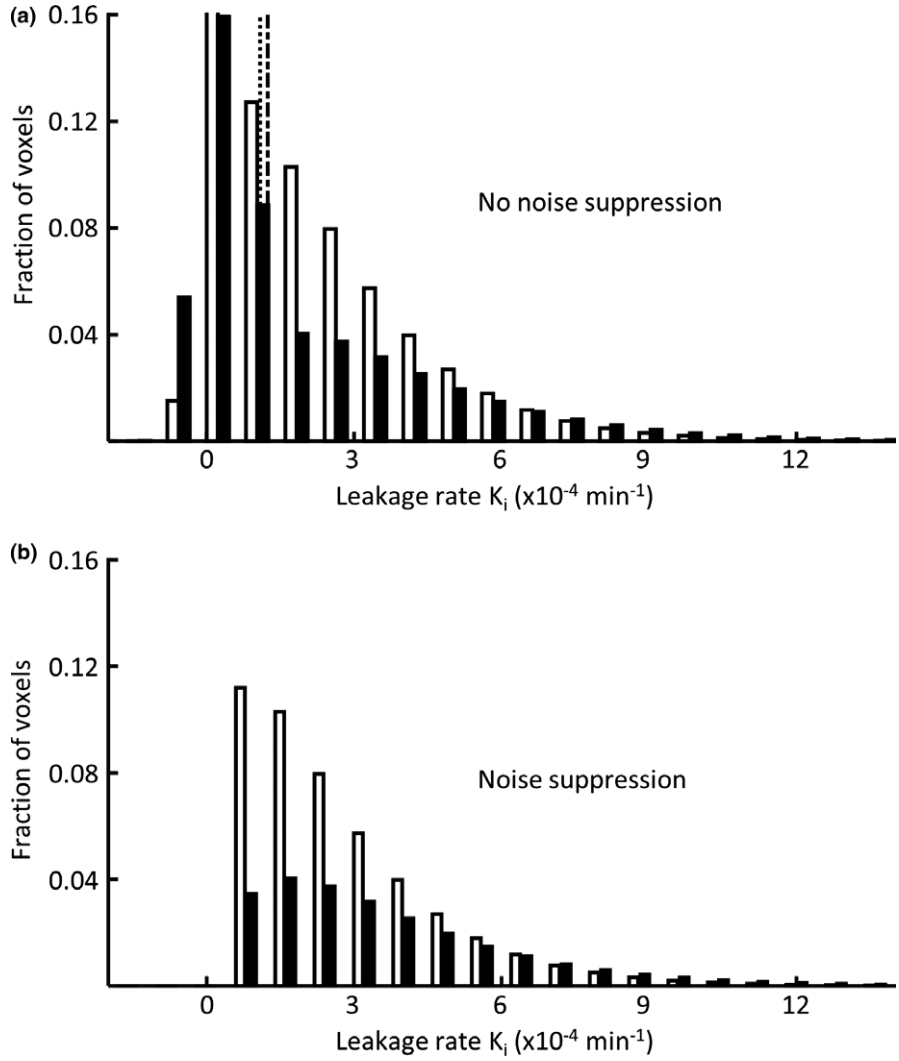

FIG. 3. An illustration of the effect of the noise suppression on two different histograms. The leakage distributions of subpanel A, which still exhibit noise and negative leakage rate values, have almost the same mean K_i (black distribution/dotted line: 1.09×10^{-4} min^{-1}, white distribution/dash-dotted line: 1.24×10^{-4} min^{-1}) with a percentage difference of 14%, with the most notable differences in the section of the lowest K_i values. The white distribution has more low K_i values, close to the zero level, than the black distribution. After noise suppression, in subpanel B the difference between the distributions becomes more clear, showing relatively more voxels exhibiting leakage in the lowest leakage rate range for the white distribution. By calculating v_L, the sum of the bins, this difference becomes quantitatively apparent, revealing a much higher percentage difference of 105% between the two distributions (black: 0.19, white: 0.40).

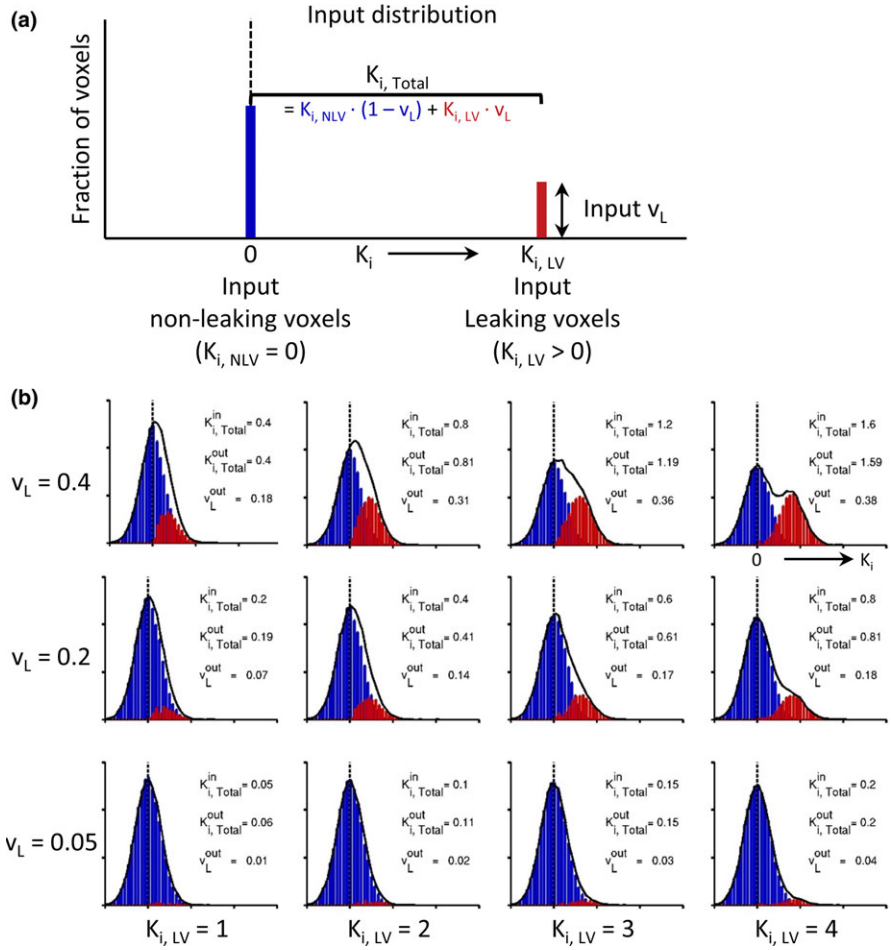

FIG. 4. Simulations illustrating the behavior of K_i and v_L when altering the ratio nonleaking ($K_i = 0$) and leaking ($K_i > 0$) voxels together with varying the leakage rate (K_i). The basic input distribution is shown in A. In brief, the voxels were divided into a nonleaking (1-v_L) and leaking (v_L) fraction. The fraction of the leaking voxels (input v_L) and leakage rate ($K_{i,\,LV}$) was varied to create the different input distributions of nonleaking (blue bins) and leaking (red bins) voxels. After adding noise to the concentration curves (for details, see the Methods section), the K_i values were recalculated and the resulting histogram was analyzed in the way described in the text. The $K_{i,\,Total}$ displayed in the graphs combines the K_i of the nonleaking and leaking voxels into the total distribution (denoted by the black curve), which is equal to $K_{i,\,Total} = v_L \cdot K_{i,\,LV}$ (because $K_{i,\,NLV} = 0$). The figure shows that the measured (total) K_i is not equal to the (input) $K_{i,\,LV}$ of the leaking voxels. It also demonstrates that the relative volume of leaking voxels v_L is more accurately measured when either the relative amount of leaking voxels or the leakage rate of the leaking voxels increases. For these simulations, a scan time of 15 min and a signal-to-noise ratio of 1.68 was used. All K_i values are $\times 10^{-4}$ min^{-1}.

in the NAWM and cortex. Statistical significance was inferred when $P < 0.05$.

To determine how shortening of the scan time affects K_i and v_L, the statistical tests were repeated for shorter scan times by discarding the data beyond that time. For example, for a scan time of 10 min, the Patlak plot of each relevant voxel was constructed with data obtained from t = 0 to 10 min.

2.F. Sample size estimation

The imaging data also allowed for a post hoc power analysis, which was used to estimate the impact of group size and scan time on the statistical power. We used the measured effect and standard deviation as a function of scan time in both the NAWM and cortex over the subjects to calculate the 80% power levels for different effect sizes and group sizes using $N \approx 2\sigma^2 \left(Z_\alpha + Z_{1-\beta}\right)^2 / \Delta^2$, where the Z-scores correspond to the critical statistical significance level α and power $1-\beta$. Here, N is the group size, σ is the pooled standard deviation over the subjects, Δ is the (absolute) mean difference in K_i or v_L between the groups (i.e., effect size), α is the probability of a type I error (set at 5%), and β is the probability of a type II error (the power, $1-\beta$, set at 80%).[26] Smaller effect sizes were expressed as a fraction of the measured effect size, that is, an effect size of $0.75\Delta v_L$ indicates that the difference in v_L between the patients and controls was reduced by 25%. The difference between the mean of the patients and controls, Δ, was based on the imaging data and thus depended on the scan time. These calculations served to indicate the relation between group size and scan time, and the effect on the power for various Δ values.

2.G. Simulations

To further investigate the effect on the measured K_i and v_L when the scan time is shortened, computer model simulations

of concentration time-curves were performed using Matlab. A VIF was calculated from the mean blood curve data of the controls by fitting a linear curve to the arrival phase, and a biexponential curve to the washout phase of the contrast agent concentration time-course.[27] CNR's were calculated from the concentration curves in the white matter of the control subjects (CNR = mean/standard deviation from t = 20 to 25 min) and used to introduce random noise to the simulated tissue concentration time-curves. To simulate realistic K_i values of the region of interest (ROI), a Pareto distribution was used to provide input K_i values, as previously described by Taheri et al.[13] Although the true BBB leakage distribution is unknown due to the absence of a golden standard, we consider the Pareto distribution a reasonable model as it comprises a long tail combined with a relatively high fraction of voxels with subtle K_i values. It is given by the formula

$$f(x) = \frac{ab^a}{x^{a+1}} \quad \text{for} \quad x \geq b$$

where f(x) gives the relative incidence of a K_i value (x) and a and b define the shape and scale of the distribution, respectively. We varied a and b to examine different leakage histograms. Note that only positive K_i values were included for the input. Next, the K_i values from the distribution were converted to concentration time courses, using pharmacokinetic modeling with the fitted VIF and an assumed v_p. Noise was added to these curves and the K_i and v_p measures were recalculated in the same way as the *in vivo* data for each simulated voxel. This was repeated for scan times increasing from 5 to 25 min. We used the CNR (1.68) and v_p (0.005, comparable to other studies) of the NAWM.[3,6] The CNR was determined from the measured concentration curves of the control subjects. A near-constant concentration was assumed after 20–25 min, and the CNR was calculated by the ratio of the mean concentration and the standard deviation. The CNR value was used to introduce random noise to the simulated concentration curves. The NAWM was chosen because BBB leakage is suggested as one of the earlier mechanisms of white matter degeneration, and the measurement of contrast leakage is expected to be more challenging due to the lower blood perfusion compared with the cortex.[3,28] The distributions consisted of 90 K voxels (180 cm^3), which is comparable to the NAWM volume.

3. RESULTS

Examples of the concentration curves of single voxels with a low and a high K_i, with the corresponding individual VIF and the resulting Patlak plots are provided in Fig. 5. In the NAWM, the patients had a median K_i of 0.75×10^{-4} (standard deviation, s.d. 0.46×10^{-4}) min^{-1} and the healthy controls had a slightly lower value of 0.70×10^{-4} (s.d. 0.63×10^{-4}) min^{-1} after 25 min of scan time. This difference was not significant ($P = 0.8$). In the cortex, the patients had a higher median K_i of 1.04×10^{-4} (s.d. 1.24×10^{-4}) min^{-1} compared with 0.08×10^{-4} (s.d. 0.76×10^{-4}) min^{-1} in the control subjects after 25 min of scan time. This difference was significant ($P = 0.014$), and remained significant until the scan time was shortened to less than 14.5 min of scan time (Fig. 6).

Both the *in vivo* measurements and simulations showed that the observed median K_i will decrease with scan time (Figs. 6 and 7). Further examination of the simulations revealed that at longer scan times, the K_i distribution histogram became more skewed towards higher K_i values, that is, the upper tail of the distribution. The decreasing influence of noise results in a decrease of the median K_i, as less (noisy) voxels are present in the upper tail. The simulations also revealed that even though the measured K_i decreases with increasing scan time, the true (i.e., input median) K_i is not reached within a scan time of 25 min (Fig. 7). To show the effect of SNR on the K_i estimation, we also performed simulations with different SNR but fixed scan time and input K_i. The results of these simulations are displayed in Fig. 8.

The patients exhibit a significantly higher v_L compared with the controls in both the NAWM (patients: 0.41, s.d. 0.17, controls: 0.27, s.d. 0.13, $P = 0.018$) and cortical gray matter (patients: 0.31, s.d. 0.22, controls: 0.15, s.d. 0.10, $P < 0.01$) at 25 min scan time. We also found that v_L decreases with increasing scan time (Fig. 6).

Leakage maps of a representative patient obtained at different scan times are displayed in Fig. 9. As can be appreciated from Fig. 6, 15.5 minutes of total scan time is the minimum to obtain a statistically significant (i.e., $P < 0.05$) difference in v_L between the patient (0.52, s.d. 0.04) and control group (0.42, s.d. 0.03) in the NAWM. Only 8 min are required in the cortex (patients: 0.58 s.d. 0.06, controls: 0.42 s.d. 0.04), and $P < 0.01$ after 12.5 min.

Based on the *in vivo* imaging data, the balance between required group sizes and scan times for a constant statistical power of 80% was calculated. The depicted relation allows for an estimation of the group sizes and scan time given a certain K_i or v_L difference. The difference in K_i in the NAWM was not significant at any investigated scan time, and the power was quite low (power of 8% at 25 (0.42, s.d. 0.03) in the NAWM. Only 8 min are required in the cortex (patients: 0.58 s.d. 0.06, controls: 0.42 s.d. 0.04), and $P < 0.01$ after 12.5 min. power of the effect in the NAWM is 85%. In the cortex, the current study reaches a power of 98%. This indicates that the current study had sufficient (statistical) power to find the difference for v_L in the NAWM, but shortening the scan time or decreasing the group size would result in the study being underpowered. To measure the effect in the cortex, our data show that 80% power can still be achieved if the scan time would be lowered to 15 minutes, or the group size would be decreased to 9 (Fig. 10). However, the current study has 84% power at $0.75\Delta v_L$, and further shortening of scan time or lowering group size with such an expected effect size will cause the power to fall below the 80% level.

4. DISCUSSION

A number of ways to improve the sensitivity of DCE-MRI to detect widespread subtle BBB leakage were investigated in

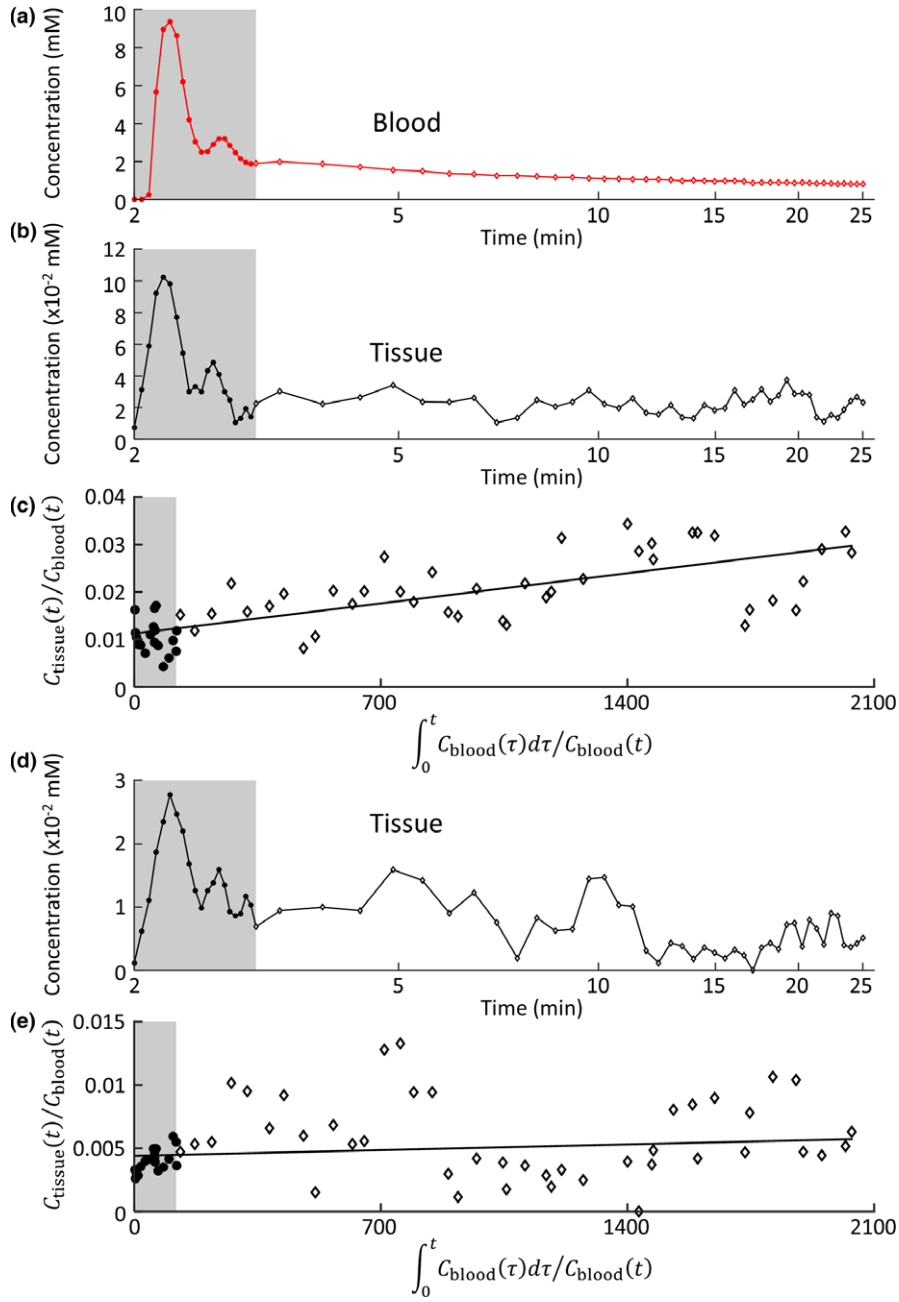

FIG. 5. Contrast agent concentration time curves in a blood vessel (a) and in tissue (b) and (d). The Patlak plots resulting from combining the tissue curves with the blood curve, are given (c) and (d). This resulted in a relatively high K_i (c) and a lower K_i value (d). The voxels were selected in the normal appearing white matter of a single patient with early Alzheimer's disease. The gray background and filled markers indicate when the fast protocol was used. While the Patlak plot in C shows a clear upwards trend, resulting in a K_i of 5.4×10^{-4} min^{-1} (standard error, s.e. 1.1×10^{-4} min^{-1}) and a $v_p = 1.1\%$ (s.e. 0.18%), the Patlak plot in E shows a much less coherent pattern, resulting in a K_i 0.4×10^{-4} min^{-1} (s.e. 0.34×10^{-4} min^{-1}) and a $v_p = 0.4\%$ (s.e. 0.06%). A slight change in the points of E may cause the slope of the Patlak plot to become negative leading to the measurement of a negative K_i, which illustrates the need for a method to reduce the impact of noise. [Color figure can be viewed at wileyonlinelibrary.com]

patients with early AD. *In vivo* imaging data showed that the (median) leakage rate K_i is strongly influenced by noise, and that both the observed K_i and fraction of leaking tissue v_L decrease for longer scan times. Based on the *in vivo* imaging data, we also calculated the scan time and group size needed for different effect sizes.

DCE-MRI has been used in tumors with success, but applications in neurodegenerative diseases are more difficult. In part, this difficulty can be attributed to the spatial distribution of the leakage. In tumors, increased contrast agent leakage is usually localized in the tumor tissue.[29] However, the leakage may be much more widespread in neurodegenerative diseases. Although voxelwise mapping of leakage may be an appropriate approach to detect widespread leakage, it is also more susceptible to noise compared with region-of-interest approaches. Furthermore, where in tumors the leakage rate

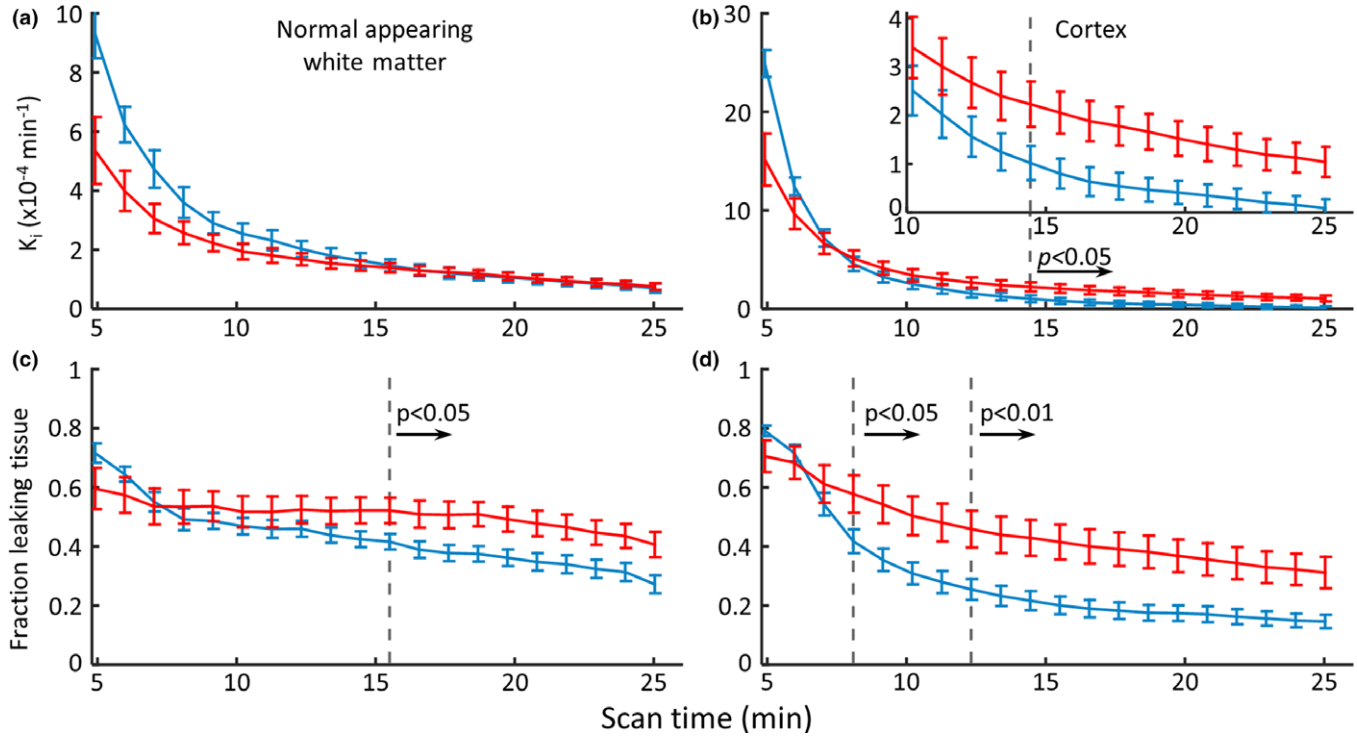

FIG. 6. Median K_i of the normal appearing white matter and cortical gray matter of the patients and controls (a) and (b), and fraction leaking tissue (v_L) (c) and (d) versus scan time. The error bars denote the standard error of the mean. The vertical dashed lines show the scan time at which a significant difference in the fraction of leaking tissue was found between the groups. The second graph in B shows a magnification of the same data in the cortex, to better demonstrate the differences between the groups. As with the simulated data, K_i decreases with scan time (a) and (b). Furthermore, v_L also decreases with scan time (c) and (d).

may be the most important measure, there is no reason to assume that hotspots of high leakage exist in neurodegenerative diseases such as AD. The commonly used mean K_i in a region may not be the most appropriate measure for an increase in leakage extent rather than rate (i.e., strength). This prompted us to develop the volume of detectable leakage v_L. However, future studies may look into other possible ways to measure leakage extent. For example, in functional MRI, approaches based on clustering or independent component analysis have been successfully applied to increase sensitivity to more subtle signal changes due to cortical activation.[30,31] Similar methods may also be useful in DCE-MRI experiments in neurodegenerative diseases.

The effect of noise on the K_i distribution changes with scan time, because for longer scan times the impact of noise on the concentration curves is reduced. This is due to the increased number of measurements (time-points) and because the contrast agent has more time to extravasate, resulting in higher extravascular concentrations which are easier to detect. The upper tail of the (skewed) distribution, containing the higher and more relevant voxelwise K_i values, becomes more apparent (see also Fig. 4). Concomitantly, the number of high values that can be attributed to noise are reduced and the noise values in general become more concentrated around zero. On the contrary, for decreasing scan times, the measured concentration-time curves become increasingly dominated by noise, leading to a stronger variation of slope values in the Patlak plots. At shorter scan times the resulting K_i histograms are broad and nearly symmetric, with a peak at a positive K_i value (due to the skewed input distribution). At such short scan times, actual leakage cannot be distinguished from noise. The skewed input distribution causes the median K_i to decrease with longer scan times. The v_L also decreases for longer scan times. This is also caused by the decreasing influence of the noisy values in the upper tail of the distribution, causing a larger fraction of voxels to be attributed to noise, lowering the calculated v_L.

The subtle leakage profiles found in this study are comparable to previously reported values in neurodegenerative disease, which are as low as 10^{-4} min^{-1}.[6,12,13,15,32,34] The *in vivo* data show that detecting differences between a group of patients with a neurodegenerative disease and a control group is feasible. However, if the effect is somewhat smaller than what we measured (e.g., $0.75\Delta v_L$), the detection of differences becomes more difficult, especially in the white matter. If the difference between the patient and control groups is only half of the original effect ($0.5\Delta v_L$), the required scan time and group size increase considerably, making such studies more challenging.

The simulations show an overestimation of K_i, which is still present at scan times up to 25 min (Fig. 4). The median K_i observed in the *in vivo* data is also below the detection limit of $10{\cdot}10^{-4}$ min^{-1} previously reported by Cramer and Larsson.[6] This suggests that determining the absolute K_i

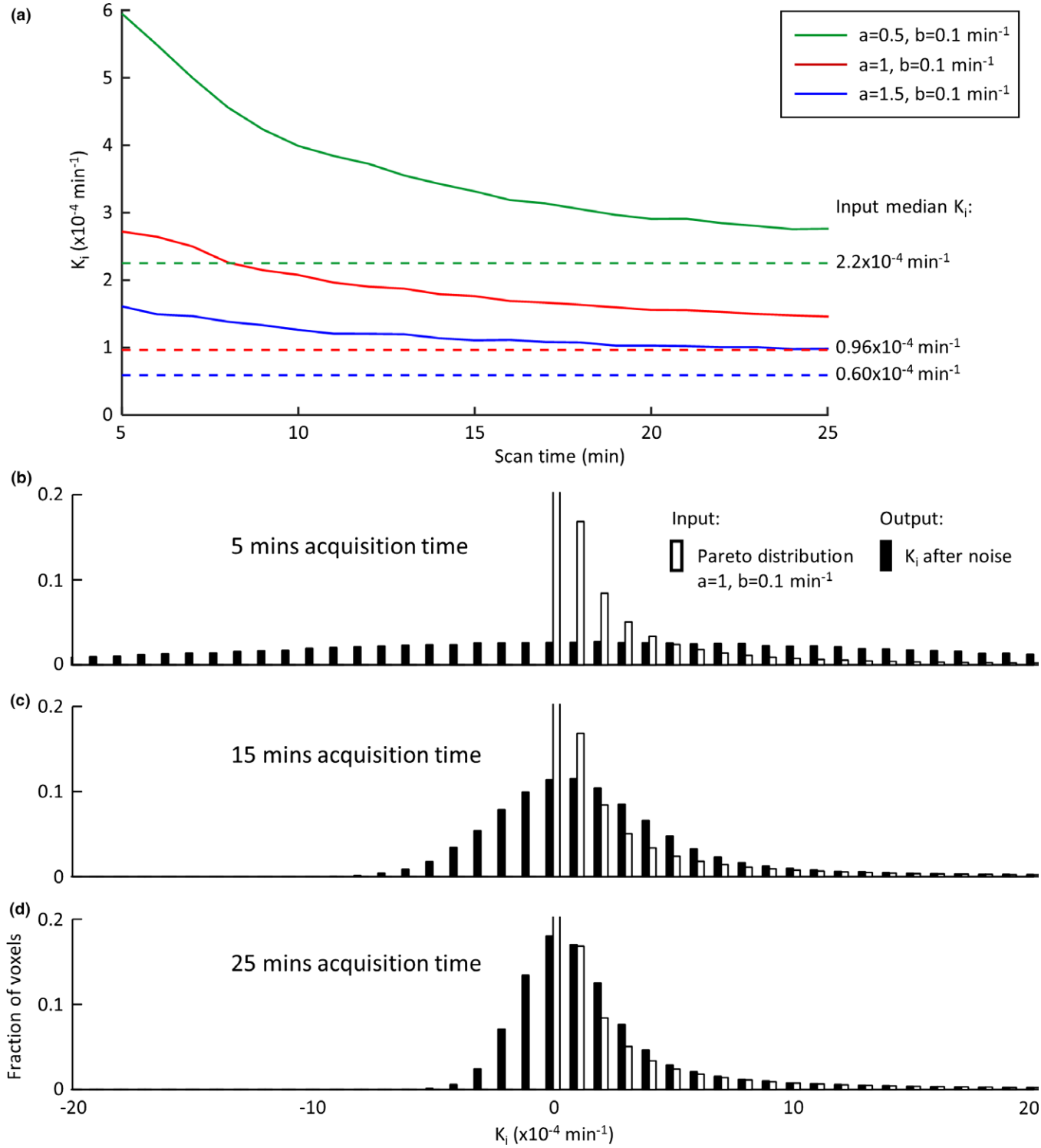

FIG. 7. The median K_i of the simulated data versus scan time using different input distribution parameters (a) and K_i distributions calculated in the simulations for various scan times (b), (c) and (d). The dashed lines in A indicate the median K_i of the profile used as input for the simulations. K_i decreases with increasing scan time. The simulations also show that the measured K_i is biased, as the input K_i (dashed lines) is not reached, even after 25 min of scan time. This bias is 66% for the K_i profile with the lowest input median (blue) and 23% for the profile with the highest input median (green). The histograms show the effects of changing the scan time in more detail. The K_i distribution after noise was added to the concentration-time courses, with a scan time of 5 min (b), shows a wide range of K_i values. There is no discernable tail at the higher K_i values as is shown in the input distribution. A longer scan time (c) reduces the influence of noise and the tail of the K_i distribution containing the relevant values becomes better delineated, which continues at longer scan times (d).

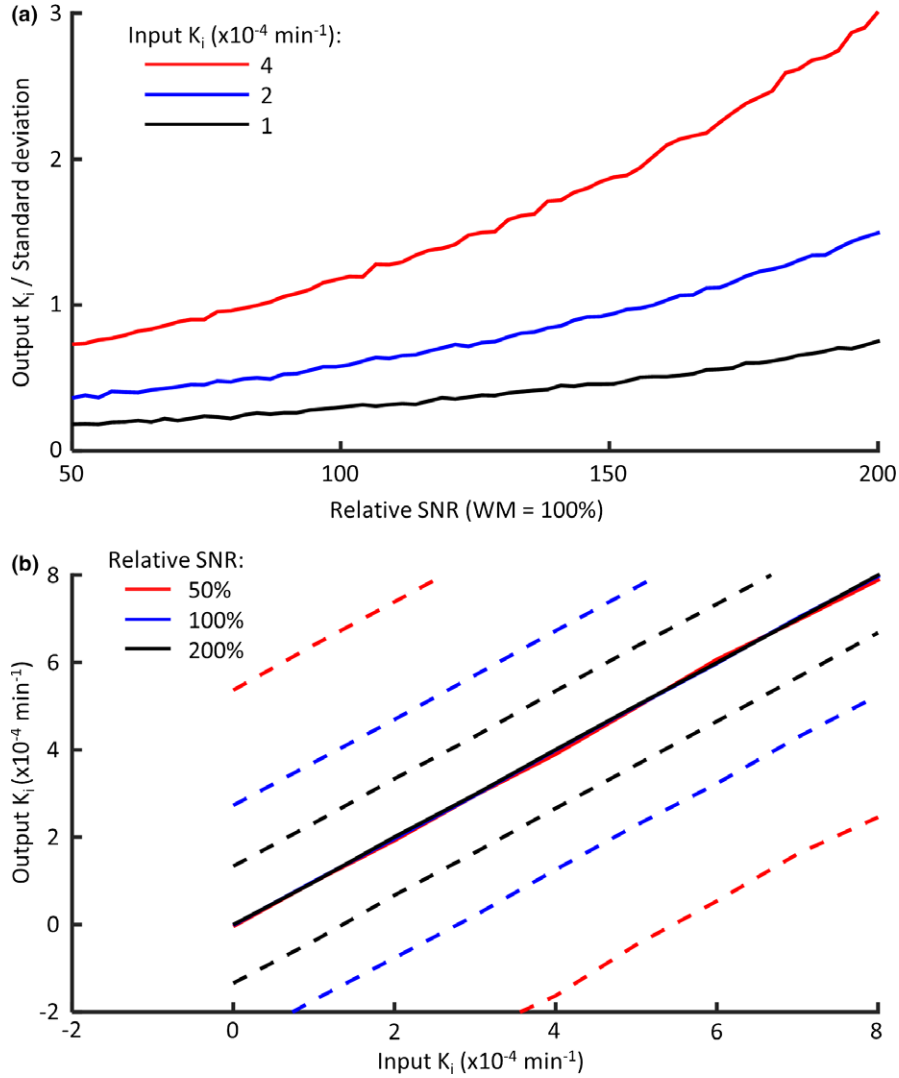

FIG. 8. S!imulations showing the effect of the signal-to-noise ratio (SNR) on the accuracy of the K_i estimation. The SNR was scaled relative to the SNR found in the white matter (WM) of the *in vivo* measurement, which was 1.68. Figure A shows the output K_i relative to the standard deviation versus the noise level, while B shows the effect of various noise levels on different input K_i values.

value accurately seems not feasible given the lower leakage values found in this study. This notion hampers direct comparison of leakage rate values between studies, as the K_i values strongly depend on the scan time and noise level. To obtain a representative alternative measure for BBB leakage per participant, we proposed v_L. This measure proved more sensitive to the relatively larger number of subtly leaking voxels in the patients with early AD compared with the controls.

Given that DCE-MRI is most commonly used in oncology, scan times are often based on much higher K_i values than found in neurodegenerative disease. For example, Aerts et al. found that scan times beyond 7 min did not further improve leakage estimates in tumor tissue.[25] However, this was established assuming a (tumor) leakage value of 0.1 min^{-1}, which is three orders of magnitude higher than the currently observed values in early AD ($K_i \approx 1 \times 10^{-4}$ min^{-1}). A recent study showed the effect of scan time on the contrast-to-noise ratio of the leakage rate K^{trans} (where $K_i = K^{trans}/(1-\text{hematocrit})$.[11] They concluded that the most optimal scan time depended on the value of K^{trans}. Longer scan times provide a more precise value, but also give more time for the contrast agent to return back into the blood (reflux), which is assumed to be negligible in the Patlak model. The leakage rates found in our *in vivo* data, are much lower than those reported by Barnes et al. (approximately 20×10^{-4} min^{-1} after hematocrit correction). They reported that such subtle leakage strongly decreases the influence of reflux. On the other hand, the influence of noise becomes quite strong for such low leakage values, which is the central topic of the current study. Cramer and Larsson have also investigated the requirements for measuring subtle BBB leakage, and focused on the pharmacokinetic model and the sampling frequency.[6] Concerning the scan time, they show that increasing the scan time decreases the influence of noise, which manifests itself as a low standard deviation on the

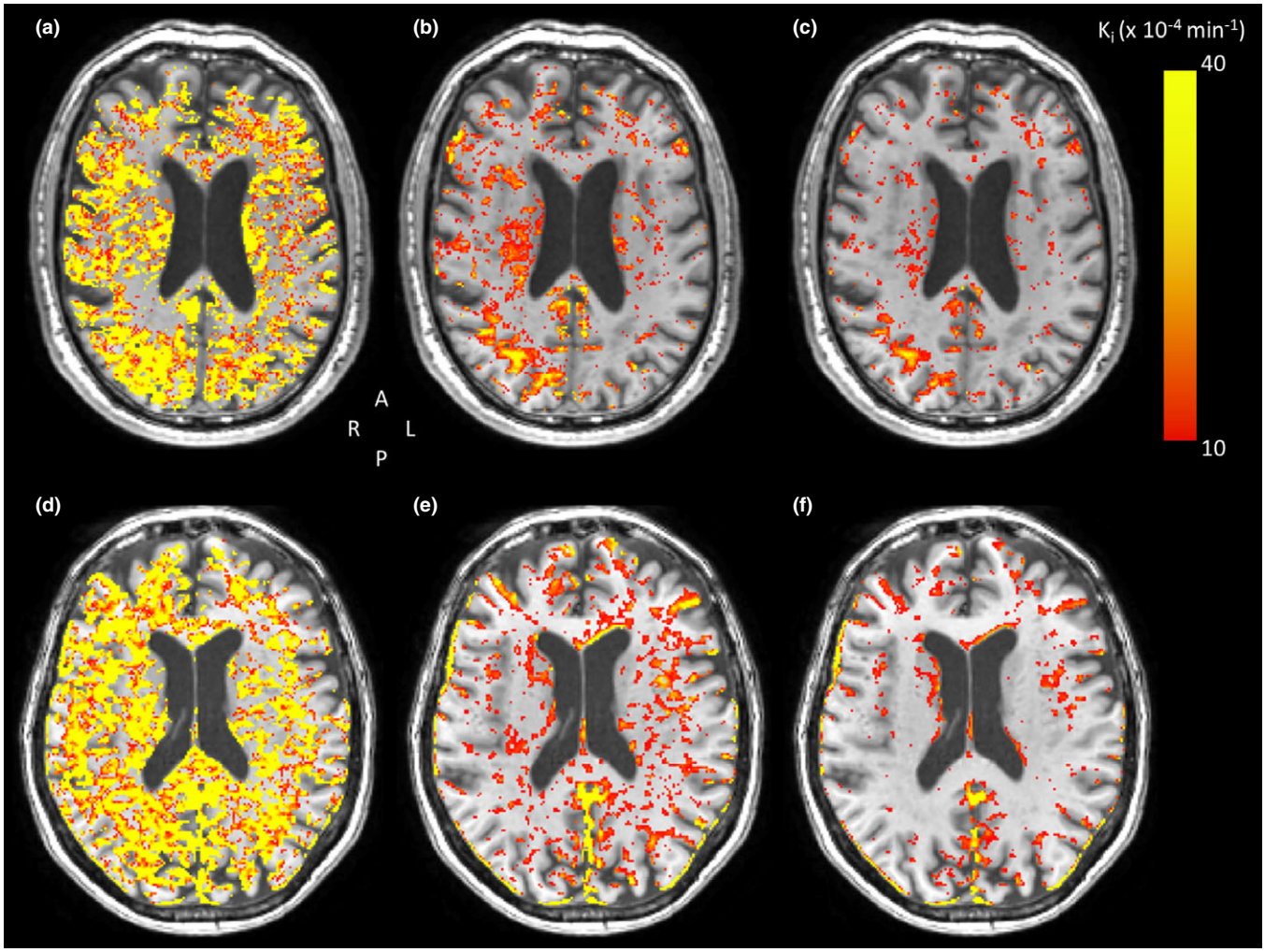

FIG. 9. Overview of the leakage maps of a patient (a)-(c)and a control (d)-(f), superimposed on the T1-weighted image, at 5 (a) and (d), 15 (b) and (e) and 25 (c) and (f) minutes of scan time. Note that voxels with a K_i value below the cutoff of 10×10^{-4} min^{-1} are not shown to focus on the higher and more relevant K_i values. Images (a) and (c) show that the voxels have a wide range of K_i values at 5 min of scan time, but these are heavily influenced by noise. A longer scan time reduces the absolute K_i values (as seen by the transition from yellow to red in (b) and (e) and less high K_i voxels are displayed, while more voxels fall below the threshold of 10×10^{-4} min^{-1}. At 25 min of scan time (c) and (f), the impact of noise is reduced further, and more voxels fall below the display threshold, while higher K_i voxels become more sparse but also more meaningful.

estimated K_i, but has no or negligible impact on the magnitude of K_i. There are two important methodological aspects worth comparing this study to that of Cramer and Larsson. First, we used a dual time resolution DCE-MRI protocol. The high temporal resolution in the study of Cramer and Larsson should prevent undersampling of the VIF, similar to the high temporal resolution part of the dual time resolution protocol.[17] If a lower temporal resolution would be used, the undersampling of the VIF would cause the K_i to be overestimated, resulting in faulty leakage estimates.[17,25] The dual time resolution sequence also allows for a higher SNR during the long washout of the contrast agent, which may improve the leakage estimation. Second is the use of a K_i histogram to simulate the effects of a DCE-MRI experiment, whereas Cramer and Larsson used the more common Monte Carlo approach of single voxel K_i values. We feel that the histogram more closely simulates the combination of variations and noise in maps of (very low) K_i values, which way provides novel insights into the consequences of varying the scan time.

The necessary scan time can also be influenced by other methodological choices, such as the choice of contrast agent and the pharmacokinetic model.[6,16,33–35] The intrinsic properties of the contrast agent such as lipophilicity, charge and size, determine how easily it may pass the BBB.[36] If a new contrast agent would be developed that can pass the BBB more easily, the subtle signal differences on MRI would be larger. This would make it easier to measure the leakage, which may translate to a shorter scan time. For the pharmacokinetic model we chose to use the Patlak plot to quantify the leakage, as this was previously shown to be the best approach for subtle leakages when the reflux can be ignored.[6,11] Different models require different scan times,

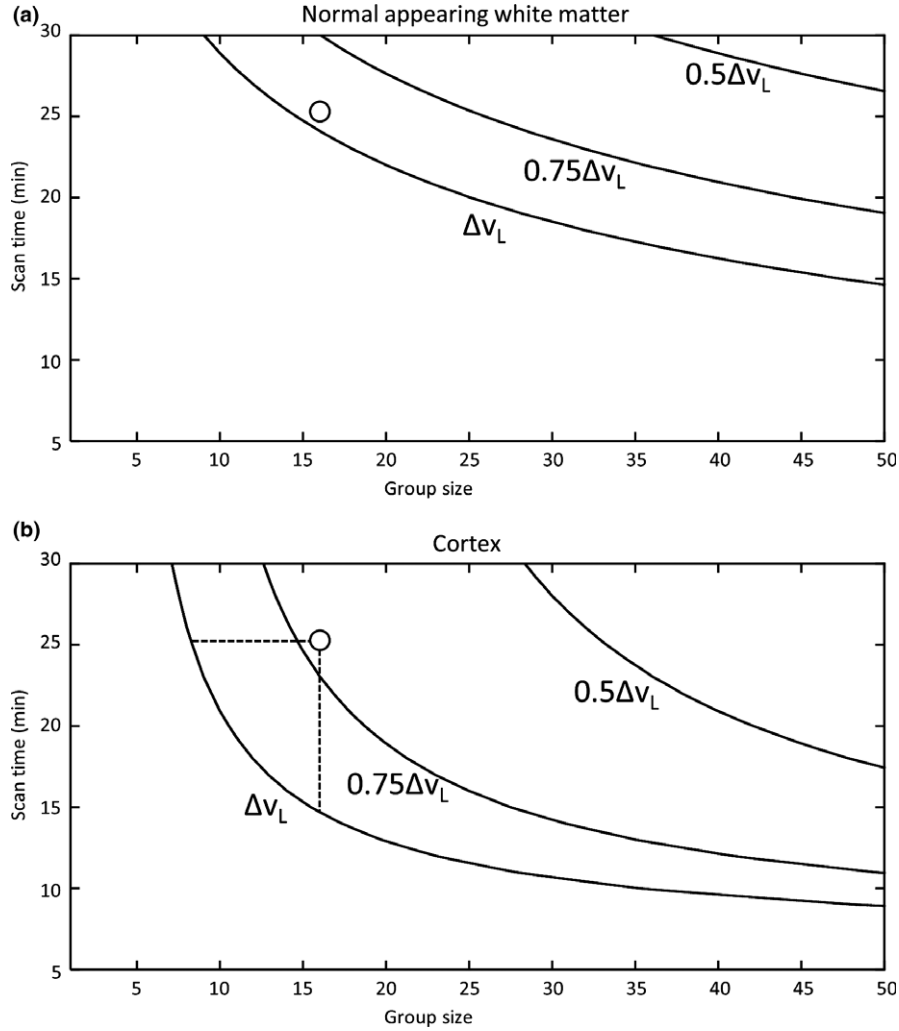

FIG. 10. The relation between scan time and group size in the normal appearing white matter (NAWM) (a) and cortex (b) at a constant power level of 80%. Δv_L is the difference in the fraction of leaking tissue between the patients and the controls. The power contours for different effect sizes are shown ($0.5\Delta v_L$ means that the difference between the patients versus the controls is half of the measured difference from the imaging data). The circles denote the current study. The graph shows that 80% power could still be achieved in the cortex by decreasing the group size to 9 (following the dashed line to the left), or decreasing the scan time to 15 minutes (following the dashed line downwards). However, the current group size and scan time are appropriate if the effect size would be smaller ($0.75\Delta v_L$) or if, instead of the cortex, the NAWM is of interest.

depending on the underlying assumptions of the model.[11] Furthermore, we note that the current noise correction approach is data-driven and does not make use of analytical models of the noise distribution. An elegant future approach would be to view the measured K_i histogram as a convolution of the actual K_i histogram and a noise kernel (model, for instance Gaussian) function, which broadens the actual K_i distribution. The deconvolution operation could then be applied to reconstruct the actual K_i distribution. The advantage of this convolution approach is that no parts of the K_i histogram need to be approximated as noise, though a model for the noise function needs to be determined. Besides these methodological considerations, it is also important to consider the impact of a long scan time on the subject. It is common that a patient with a neurodegenerative disease has some form of cognitive impairment, which would increase the burden of an MRI experiment compared with a healthy control subject.

5. CONCLUSIONS

We have introduced the leakage volume v_L, which appears more suitable and time-efficient than leakage rate K_i to detect subtle BBB leakage differences between patients with early AD and controls. Compared with K_i, v_L is a measure for the spatial extent of the leakage rather than the leakage strength. Computer simulations, showing how the measured leakage is affected by changing the scan time, and statistical power calculations were used to help to improve methodological study design. Overall, this information should assist future research aimed at investigating the subtle BBB leakage in neurodegenerative diseases.

ACKNOWLEDGMENTS

This study was performed with support from the "Internationale Stichting Alzheimer Onderzoek" (ISAO, grant 10553).

CONFLICTS OF INTEREST

The authors have no relevant conflicts of interest to declare.

[a)]Author to whom correspondence should be addressed. Electronic mail: w.backes@mumc.nl.

REFERENCES

1. Erickson MA, Banks WA. Blood-brain barrier dysfunction as a cause and consequence of Alzheimer's disease. *J Cereb Blood Flow Metab*. 2013;33:1500–1513.
2. Wardlaw JM, Smith C, Dichgans M. Mechanisms of sporadic cerebral small vessel disease: insights from neuroimaging. *Lancet Neurol*. 2013;12:483–497.
3. Sourbron S, Ingrisch M, Siefert A, Reiser M, Herrmann K. Quantification of cerebral blood flow, cerebral blood volume, and blood-brain-barrier leakage with DCE-MRI. *Magn Reson Med*. 2009;62:205–217.
4. Zlokovic BV. The Blood-Brain Barrier in Health and Chronic Neurodegenerative Disorders. *Neuron*. 2008;57:178–201.
5. Larsson HBW, Courivaud F, Rostrup E, Hansen AE. Measurement of brain perfusion, blood volume, and blood-brain barrier permeability, using dynamic contrast-enhanced T1-weighted MRI at 3 tesla. *Magn Reson Med*. 2009;62:1270–1281.
6. Cramer SP, Larsson HBW. Accurate determination of blood-brain barrier permeability using dynamic contrast-enhanced T1-weighted MRI: a simulation and in vivo study on healthy subjects and multiple sclerosis patients. *J Cereb Blood Flow Metab*. 2014;34:1655–1665.
7. Khalifa F, Soliman A, El-Baz A, et al. Models and methods for analyzing DCE-MRI: a review. *Med Phys*. 2014;41:124301.
8. van de Haar HJ, Burgmans S, Hofman PAM, Verhey FRJ, Jansen JFA, Backes WH. Blood-brain barrier impairment in dementia: current and future in vivo assessments. *Neurosci Biobehav Rev.* 2015; 49C:71–81.
9. Starr JM, Farrall AJ, Armitage P, McGurn B, Wardlaw JM. Blood-brain barrier permeability in Alzheimer's disease: a case-control MRI study. *Psychiatry Res - Neuroimaging*. 2009;171:232–241.
10. Armitage PA, Farrall AJ, Carpenter TK, Doubal FN, Wardlaw JM. Use of dynamic contrast-enhanced MRI to measure subtle blood-brain barrier abnormalities. *Magn Reson Imaging*. 2011;29:305–314.
11. Barnes SR, Ng TSC, Montagne A, Law M, Zlokovic BV, Jacobs RE. Optimal acquisition and modeling parameters for accurate assessment of low K trans blood-brain barrier permeability using dynamic contrast-enhanced MRI. *Magn Reson Med*. 2016;75:1967–1977.
12. Taheri S, Gasparovic C, Huisa BN, et al. Blood-brain barrier permeability abnormalities in vascular cognitive impairment. *Stroke*. 2011;42:2158–2163.
13. Taheri S, Gasparovic C, Shah NJ, Rosenberg GA. Quantitative measurement of blood-brain barrier permeability in human using dynamic contrast-enhanced MRI with fast T1 mapping. *Magn Reson Med*. 2011;65:1036–1042.
14. Bronge L, Wahlund L-OO. Contrast-enhanced MRI of White Matter Lesions in Patients with Blood-Brain Barrier Dysfunction. *Dement Geriatr Cogn Disord*. 2000;11:477–481.
15. Montagne A, Barnes SR, Sweeney MD, et al. Blood-Brain Barrier Breakdown in the Aging Human Hippocampus. *Neuron*. 2015;85:296–302.
16. van de Haar HJ, Burgmans S, Jansen JFA, et al. Blood-brain barrier leakage in early Alzheimer's disease. *Radiology.* 2016;281:527–535.
17. Jelescu IO, Leppert IR, Narayanan S, Araújo D, Arnold DL, Pike GB. Dual-temporal resolution dynamic contrast-enhanced MRI protocol for blood-brain barrier permeability measurement in enhancing multiple sclerosis lesions. *J Magn Reson Imaging*. 2011;33:1291–1300.
18. Fischl B, Salat DH, Busa E, et al. Whole brain segmentation: automated labeling of neuroanatomical structures in the human brain. *Neuron*. 2002;33:341–355.
19. de Boer R, Vrooman HA, van der Lijn F, et al. White matter lesion extension to automatic brain tissue segmentation on MRI. *NeuroImage*. 2009;45:1151–1161.
20. Haroon HA, Buckley DL, Patankar TA, et al. A Comparison of Ktrans Measurements Obtained with Conventional and First Pass Pharmacokinetic Models in Human Gliomas. *J Magn Reson Imaging*. 2004;19:527–536.
21. Li KL, Zhu XP, Waterton J, Jackson A. Improved 3D quantitative mapping of blood volume and endothelial permeability in brain tumors. *J Magn Reson Imaging*. 2000;12:347–357.
22. Lavini C, Verhoeff JJC. Reproducibility of the gadolinium concentration measurements and of the fitting parameters of the vascular input function in the superior sagittal sinus in a patient population. *Magn Reson Imaging*. 2010;28:1420–1430.
23. Pintaske J, Martirosian P, Graf H, et al. Relaxivity of Gadopentetate Dimeglumine (Magnevist), Gadobutrol (Gadovist), and Gadobenate Dimeglumine (MultiHance) in human blood plasma at 0.2, 1.5, and 3 Tesla. *Invest Radiol*. 2006;41:213–221.
24. Patlak CS, Blasberg RG, Fenstermacher JD. Graphical evaluation of blood-to-brain transfer constants from multiple-time uptake data. *J Cereb Blood Flow Metab*. 1983;3:1–7.
25. Aerts HJWL, Jaspers K, Backes WH. The precision of pharmacokinetic parameters in dynamic contrast-enhanced magnetic resonance imaging: the effect of sampling frequency and duration. *Phys Med Biol*. 2011;56:5665–5678.
26. Zar JH. *Biostatistical Analysis*, 4th edn. Prentice Hall; 1999.
27. McGrath DM, Bradley DP, Tessier JL, Lacey T, Taylor CJ, Parker GJM. Comparison of model-based arterial input functions for dynamic contrast-enhanced MRI in tumor bearing rats. *Magn Reson Med*. 2009;61:1173–1184.
28. Wardlaw JM, Sandercock PAG, Dennis MS, Starr J. Is breakdown of the blood-brain barrier responsible for lacunar stroke, leukoaraiosis, and dementia? *Stroke*. 2003;34:806–811.
29. Choyke PL, Dwyer AJ, Knopp MV. Functional tumor imaging with dynamic contrast-enhanced magnetic resonance imaging. *J Magn Reson Imaging*. 2003;17:509–520.
30. Lee MH, Smyser CD, Shimony JS. Resting-state fMRI: a review of methods and clinical applications. *Am J Neuroradiol*. 2013;34:1866–1872.
31. Woo C-W, Krishnan A, Wager TD. Cluster-extent based thresholding in fMRI analyses: pitfalls and recommendations. *NeuroImage*. 2014;91:412–419.
32. Heye AK, Culling RD, Valdés Hernández MDC, Thrippleton MJ, Wardlaw JM. Assessment of blood-brain barrier disruption using dynamic contrast-enhanced MRI. A systematic review. *Neuroimage Clin*. 2014;6:262–274.
33. Heye AK, Thrippleton MJ, Armitage PA, et al. Tracer kinetic modelling for DCE-MRI quantification of subtle blood–brain barrier permeability. *NeuroImage*. 2016;125:446–455.
34. Cao Y, Li D, Shen Z, Normolle D. Sensitivity of Quantitative Metrics Derived from DCE MRI and a Pharmacokinetic Model to Image Quality and Acquisition Parameters. *Acad Radiol*. 2010;17:468–478.
35. Kershaw LE, Cheng HLM. Temporal resolution and SNR requirements for accurate DCE-MRI data analysis using the AATH model. *Magn Reson Med*. 2010;64:1772–1780.
36. Seelig A, Gottschlich R, Devant RM. A method to determine the ability of drugs to diffuse through the blood-brain barrier. *Proc Natl Acad Sci USA*. 1994;91:68–72.